Fuzzy robust speed controller for detuned field-oriented induction motor drive

K.H.Chao and C.M.Liaw

Abstract: The speed control performance improvement of a detuned indirect field-oriented (IFO) induction motor drive is studied. First, the dynamic behaviour of a detuned IFO induction motor drive is observed, and its transfer function model is established. Then a proportional plus integral-derivative (PI-D) two-degree-of-freedom controller (2DOFC) is designed for an ideal IFO induction motor drive for a nominal case with the desired dynamic response. As the variation of motor parameters occurs, the detuning of field-orientation accompanying the load parameter changes may significantly worsen the speed dynamic response. In this case, a compensation signal is yielded by a proposed fuzzy robust controller (FRC) in order to preserve the prescribed response. Since the compensation signal is adaptively tuned by a model following the error driven fuzzy weighting controller, and moreover, the compromise between control effort and performance is considered, the robust model following speed response is obtained. Effectiveness of the proposed controller is verified by simulation and by measured results.

1 Introduction

It is known that an indirect field-oriented (IFO) induction motor drive will behave like a separately excited DC motor if the rotor time constant used in its field-orientation scheme can be adapted online to its actual value [1, 2]. However, this is very difficult to achieve perfectly. It follows that there have been many pieces of research [2–6] emphasising in the tuning of field-orientation to pursue the ideal decoupling control, but success is still limited. For a detuned IFO induction motor drive, both its steady-state and its dynamic torque generating characteristics are degraded. This, accompanied by the variations of other system and load parameters, may result in bad outer-loop speed and position control performances. So, in the past few decades, there has also been a lot of research devoted to the application of advanced control techniques [2, 7–12] to allow the field-oriented induction motor drive to possess good and parameter-insensitive dynamic performance under wide operating ranges (e.g. the variable structure system control [7], the adaptive control [8], the fuzzy control [9], the neural networks control [10] and the robust control [11, 12]). Among these, the simple but practical robust control methods presented in [11, 12] are very effective in reducing the effects of parameter variations. However, since the weighting factor for determining the extent of disturbance compensation is fixed, the control robustness and adaptability against parameter variations are limited, in particular for a system with some nonlinearities. Thus to improve this, it is necessary to have a suitable means for online adaptively tuning the weighting factor of robust controller.

IEE Proceedings online no. 20000016

DOI: 10.1049/ip-epa:20000016

Paper first received 7th December 1998 and in revised form 12th May 1999

The authors are with the Department of Electrical Engineering, National Tsing Hua University, Hsinchu, Taiwan, Republic of China

In this paper, a fuzzy robust controller is proposed for improving the speed response of a detuned IFO induction motor drive. First, the PI-D 2DOF controller is quantitatively designed at nominal operating conditions to possess the prescribed speed tracking and regulation responses, and the closed-loop tracking transfer function, which will be used as the reference model, is derived. Then a fuzzy robust controller taking the effect of transport lag into account is developed to preserve the desired control performance in the presence of parameter variations and external disturbances. The key feature of the proposed FRC is that the weighting factor, which significantly affects the stability and control performance of the resulted system, is adaptively set by a fuzzy weighting controller. In addition the compromise between control effort and response is also considered through tuning the weighting factor automatically. Since the reference model following error is used as the input of the fuzzy controller, and the linguistic algorithms for tuning the weighting factor are properly set, more robust and better speed control performance than those of the conventional RC [11, 12] is obtained by the proposed controller.

2 Dynamic modelling of a detuned IFO induction motor drive

2.1 Ideal case

The state equations of a squirrel-cage induction motor drive in a synchronously rotating frame can be expressed as follows [1]:

$$\begin{bmatrix} v_{qs} \\ v_{ds} \\ 0 \\ 0 \end{bmatrix} = \begin{bmatrix} R_s + p\delta & \omega_e\delta & \frac{pL_m}{L_r} & \frac{\omega_e L_m}{L_r} \\ -\omega_e\delta & R_s + p\delta & \frac{-\omega_e L_m}{L_r} & \frac{pL_m}{L_r} \\ \frac{-L_m R_r}{L_r} & 0 & \frac{R_r}{L_r} + p & \omega_{sl} \\ 0 & \frac{-L_m R_r}{L_r} & -\omega_{sl} & \frac{R_r}{L_r} + p \end{bmatrix} \begin{bmatrix} i_{qs} \\ i_{ds} \\ \lambda_{qr} \\ \lambda_{dr} \end{bmatrix} \quad (1)$$

$$T_e = \frac{3}{4}P\frac{L_m}{L_r}(i_{qs}\lambda_{dr} - i_{ds}\lambda_{qr}) = T_L + B\omega_r + Jp\omega_r \tag{2}$$

where $p \triangleq d/dt$, $\delta \triangleq L_s - L_m^2/L_r$, J = total mechanical inertia, B = total damping coefficient and the meanings of other variables and parameters are clear from the literature [1].

Basically, the indirect field-orientation for an induction motor drive can be regarded as one kind of predictive control. It is found that the ideal decoupling can be achieved if the following slip angular speed command is used for making field-orientation:

$$\omega_{sl}^* = \frac{R_r i_{qs}^*}{L_r i_{ds}^*} \triangleq \frac{i_{qs}^*}{T_r^* i_{ds}^*} \tag{3}$$

where T_r^* ($\triangleq L_r/R_r$) denotes the actual rotor time constant, i_{ds}^* and i_{qs}^* are the d- and q-axes stator current commands set by the field and speed controllers. In this case, it can lead to the following three phenomena: (i) $\lambda_{qr} = 0$ and $d\lambda_{qr}/dt = 0$ (i.e. the rotor flux $\lambda_r = \lambda_{qr} - j\lambda_{dr}$ is oriented to align with the d-axis); (ii) the rotor flux can be set as $\lambda_r^* = \lambda_{dr}^* = (L_m i_{ds}^*)(1 + T_r^* s) \approx L_m i_{ds}^*$, since normally, $T_r^* << (J/B)$; and (iii) the motor developed torque is directly related to i_{qs}^* by:

$$T_e = \left(\frac{3}{4}P\frac{L_m}{L_r}\lambda_{dr}^*\right) i_{qs}^* = \left(\frac{3}{4}P\frac{L_m^2}{L_r} i_{ds}^*\right) i_{qs}^* \triangleq k_t^* i_{qs}^* \tag{4}$$

Accordingly, the torque generating capability of an ideal IFO induction motor is excellent.

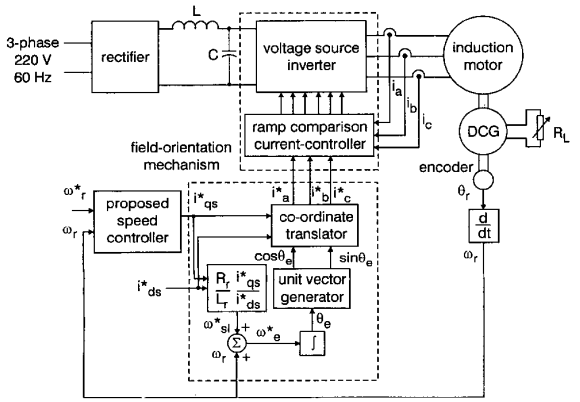

Fig. 1 *Configuration of IFO induction motor drive*

The schematic of an IFO induction motor drive with the proposed speed controller is drawn in Fig. 1. It mainly consists of a current-controlled pulse width modulated voltage source inverter (PWM VSI), an indirect field-orientation mechanism, the proposed speed controller, and an induction motor set with its rotor mechanically coupled to a DC generator. The switched load resistor R_L of the DC generator is used to change the dynamic load of induction motor. To change the inertia of the motor drive, a cylinder is mechanically attached to the motor shaft.

2.2 Detuned case

Unfortunately, the tracking of the rotor parameters employed in the indirect field-orientation mechanism according to their actual values is very difficult. This may lead to the nonideal decoupling control, and thus the torque response becomes oscillatory and sluggish. In this paper, the speed response improvement will be accomplished through applying the proposed fuzzy robust control technique. For facilitating the analysis and design of the proposed controller, a suitable model representing the dynamic behaviour of a detuned IFO induction motor drive is first built up. Since the detuning of indirect field-orientation is mainly due to the variations of rotor parameters, it is assumed that: (i) the flux current command $i_{ds}^* = i_{ds}^*$ = constant; and (ii) the varied motor parameter to be considered is T_r, and the variation from its actual value is defined to be $\Delta T_r \triangleq T_r - T_r^*$.

From eqns. 1 and 2, one can get the following small-signal differential equations using perturbation and linearisation techniques [2]:

$$p\Delta\lambda_{qr} = -(1/T_r)\Delta\lambda_{qr} - \omega_{sl0}^*\Delta\lambda_{dr} + [(L_m/T_r) - \lambda_{dr0}/(T_r^* I_{ds0})]\,\Delta i_{qs}^* \tag{5}$$

$$p\Delta\lambda_{dr} = \omega_{sl0}^*\Delta\lambda_{qr} - (1/T_r)\Delta\lambda_{dr} + [\lambda_{qr0}/(T_r^* I_{ds0})]\,\Delta i_{qs}^* \tag{6}$$

$$\Delta T_e = (3P/4)(L_m/L_r) \cdot (I_{qs0}\Delta\lambda_{dr} - I_{ds0}\Delta\lambda_{qr} + \lambda_{dr0}\Delta i_{qs}^*) \tag{7}$$

where (λ_{qr0}, λ_{dr0}, I_{qs0}, I_{ds0}, ω_{sl0}) describe the chosen steady-state operating point, and it can be found by solving the system equation listed in eqn. 1, with all time derivatives being set equal to zero.

A transfer function between the torque response and the torque command current changes can be obtained [2] from eqns. 5–7 to be:

$$\begin{aligned}\frac{\Delta T_e}{\Delta i_{qs}^*} &= \frac{3PL_m}{4L_r}\left[\frac{\alpha_1 s^2 + \alpha_2 s + (\alpha_3 + \alpha_4)}{s^2 + \alpha_5 s + \alpha_6}\right] \\ &= \frac{3PL_m}{4L_r}\lambda_{dr0}\left[\frac{s^2 + (\alpha_2/\alpha_1)s + (\alpha_3 + \alpha_4)/\alpha_1}{s^2 + \alpha_5 s + \alpha_6}\right] \\ &\triangleq k_t^* + \Delta_t(s)\end{aligned} \tag{8}$$

where:

$$\begin{aligned}\alpha_1 &= \lambda_{dr0} \\ \alpha_2 &= \frac{1}{T_r}(2\lambda_{dr0} + \lambda_{qr0}\omega_{sl0}T_r - L_m I_{ds0} + \lambda_{dr0}\beta) \\ \alpha_3 &= \frac{\omega_{sl0}}{T_r}(I_{qs0}L_m + \lambda_{qr0} + \beta\lambda_{qr0}) \\ \alpha_4 &= \frac{1}{T_r^2}(\lambda_{dr0} - L_m I_{ds0} + \beta\lambda_{dr0}) \\ \alpha_5 &= \frac{2}{T_r} \\ \alpha_6 &= \frac{1}{T_r^2} + \omega_{sl0}^2 \\ \beta &= \frac{T_r}{T_r^*}\end{aligned} \tag{9}$$

$$k_t^* = \frac{3PL_m}{4L_r}\lambda_{dr0}$$

$$\Delta_t(s) = \frac{3PL_m}{4L_r}\left[\frac{(\alpha_2 - \alpha_1\alpha_5)s + (\alpha_3 + \alpha_4 - \alpha_1\alpha_6)}{s^2 + \alpha_5 s + \alpha_6}\right] \tag{10}$$

Eqns. 8–10 show that the dynamic behaviour of a detuned IFO induction motor drive, due to the variation of T_r, can be modelled by an additive uncertainty model shown in Fig. 2.

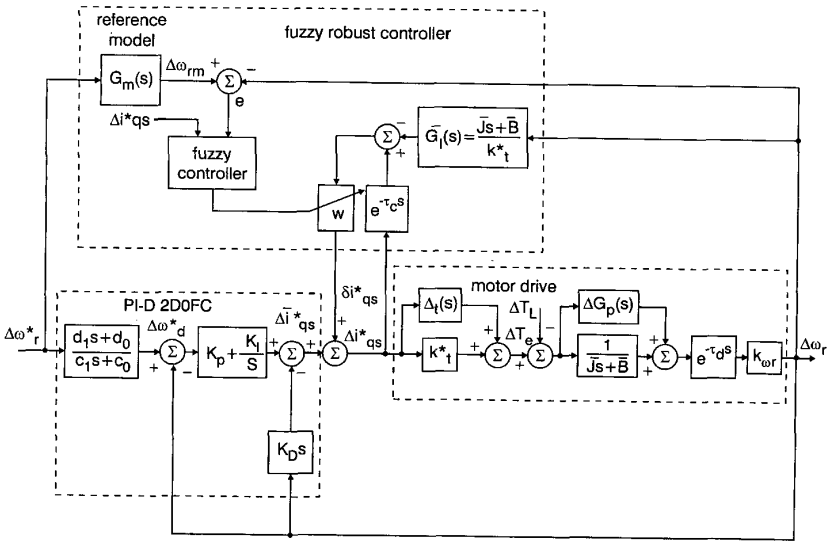

Fig. 2 *Control system block diagram of motor drive and proposed controller*

In addition to the uncertainty due to nonideal field-oriented characteristics, the mechanical parameters may also change significantly during operation, particularly the mechanical moment inertia. To consider this, the mechanical dynamic model is represented as:

$$G_p(s) = 1/(Js + B) \triangleq \overline{G}_p(s) + \Delta G_p(s) \qquad (11)$$

where:

$$\overline{G}_p(s) \triangleq \overline{b}/(s + \overline{a}) = 1/(\overline{J}s + \overline{B}) \qquad (12)$$

is the nominal mechanical model, $J \triangleq \bar{J} + \Delta J$, $B \triangleq \bar{B} + \Delta B$, and $\Delta G_p(s)$ denotes the uncertainty mechanical model. The control system block diagram of the detuned and uncertain IFO induction motor drive accompanying with the proposed controller is shown in Fig. 2, in which, $k_{\omega r}$ denotes the speed sensing factor and $e^{-\tau_d s}$ is the transport delay.

The motor used here is a three-phase Y-connected 2-pole 800W 2000 rpm 120V/5.4A motor, which has the following parameters obtained from conventional no-load and locked-rotor tests:

$$R_s = 1.1\ \Omega \quad R_r = 1.3\ \Omega$$
$$L_s = 0.144H \quad L_r = 0.144H \quad L_m = 0.136H \qquad (13)$$

The stator flux current command for rated rotor flux can be estimated as follows [13]. At steady-state operation (all derivative terms are zero), supposing that the q-axis of the synchronous rotating frame is coincident with the as-axis at $t = 0$, then $v_{qs} = \sqrt{2}V_s$ and $v_{ds} = 0$, where V_s is the RMS stator voltage in abc-domain, and the q-axis voltage eqn. 1 can be simplified to be:

$$\sqrt{2}V_s = R_s i_{qs} + \omega_e L_s i_{ds} \qquad (14)$$

The ratings of an induction servo motor generally given by the vender include: rated line-to-line voltage ($V_{l,\text{rated}}$), rated rotor speed (N_{rated}, rpm), number of poles (P), rated current and rated output power. Using these data and the measured no-load data, the d-axis current for rated flux can be found from eqn. 14 as:

$$i_{ds} = i^*_{ds} = \frac{\sqrt{2}(V_{l,\text{rated}}/\sqrt{3}) - i_{qs,NL}R_s}{L_s\omega_e}$$
$$\simeq \frac{\sqrt{2}(V_{l,\text{rated}}/\sqrt{3})}{L_s(P\pi/60)(N_{\text{rated}}/(1 - S_{\text{rated}}))} \qquad (15)$$

where $i_{qs,NL}R_s$ is neglected, owing to its small value at no load, S_{rated} is the rated slip, which can be known from the given ratings of an induction motor. Using the parameters listed in eqn. 13 and the nameplate data, the rated stator d-axis flux component current command of the induction motor is estimated from eqn. 15 to be $i^*_{ds} = 3.3$A. It can be found from eqns. 4 and 13 that $T^*_r = 0.11077$s and $k^*_t = 0.6358$. As to the nominal mechanical dynamic model, it is rather difficult to obtain, since the mechanical parameters $\bar{J}$ and $\bar{B}$ are not available generally. Thus at the chosen nominal operating condition ($\omega_{ro} = 1000$rpm, $R_L = 77.6\Omega$), the nominal plant parameters are found using the estimation technique [14] to be $\bar{a} = 0.567$, $\bar{b} = 70.68$ and $\tau_d = 0.02$s. The speed sensing factor is set as $k_{\omega r} = 0.00955$V $\cdot$ s/rad here. It follows from eqn. 12 and Fig. 2 that $\bar{J} = 0.014148\,\text{N}\cdot\text{m}\cdot\text{s}^2$ and $\bar{B} = 0.008022\,\text{N}\cdot\text{m}\cdot\text{s/rad}$, or $\bar{J} = 1.4815\,\text{N}\cdot\text{m}\cdot\text{s}\cdot\text{rad/V}$ and $\bar{B} = 0.84\,\text{N}\cdot\text{m/V}$. At the chosen nominal case ($\omega_{r0} = 1000$rpm, $R_{L0} = 77.6\Omega$, $i^*_{ds} = 3.3$A), the torque current command is measured to be $i^*_{qs} = 1.1$A. Based on these values, all the quantities at operating point are found to be (λ_{qro}, λ_{dro}, $I_{qso} = i^*_{qs}$, $= I_{dso} = i^*_{ds}$, ω_{slo}) = (0 web, 0.4488 web, 1.1A, 3.3A, 3.01rad/s).

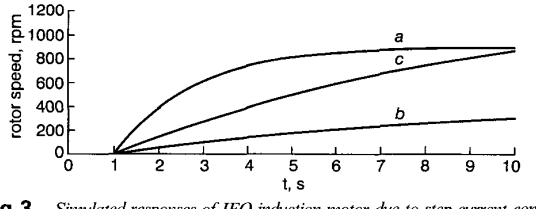

Fig. 3 *Simulated responses of IFO induction motor due to step current command change $i^*_{qs} = 1A$*
Rotor speeds
a, $T_r = 1.0\ T^*_r$, $J = \bar{J}$, $B = \bar{B}$
b, $T_r = 0.5\ T^*_r$, $J = 5\bar{J}$, $B = \bar{B}$
c, $T_r = 2.0\ T^*_r$, $J = 5\bar{J}$, $B = \bar{B}$

With a step torque current command change from 0 to 1A, the simulated rotor speeds and developed torques for several values of T_r/T^*_r and $J/\bar{J}$ are shown in Figs. 3 and 4. The results indicate that the speed and torque responses are

significantly affected by the variations of rotor and mechanical parameters.

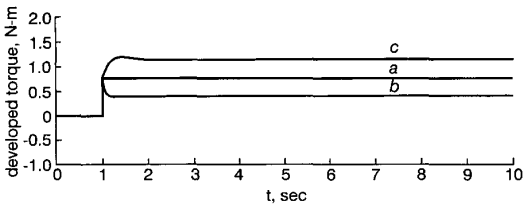

Fig. 4 *Simulated responses of IFO induction motor due to step current command change $i_{qs}^* = 1A$*
Developed torques
a, $T_r = 1.0\ T_r^*$, $J = \bar{J}$, $B = \bar{B}$
b, $T_r = 0.5\ T_r^*$, $J = 5\bar{J}$, $B = \bar{B}$
c, $T_r = 2.0\ T_r^*$, $J = 5\bar{J}$, $B = \bar{B}$

3 Proposed controller

In the proposed control system shown in Fig. 2, the 2DOFC is designed for the ideal field-oriented induction motor drive at the chosen nominal operating point according to the prescribed tracking and regulating drive specifications and the fuzzy robust controller is used to compensate for the effects of detuning of field-orientation and the variations of mechanical parameters on the speed dynamic response.

3.1 Design of the PI-D 2DOF speed controller

The PI-D 2DOFC shown in Fig. 2 consists of a PI-D controller and a command feedforward controller. In its design stage, neglecting the dead time element and the uncertainty models $\Delta_I(s)$ and $\Delta G_p(s)$, the following speed control specifications are specified.

3.1.1 Step command tracking response ($\Delta\omega_r^* = 100$ rpm):

(i) response time $t_{re} = 0.2$s, which is defined as the time for the response to rise from zero to 90% of its final value;

(ii) overshoot = 0;

(iii) steady-state error = 0;

(iv) maximum value of control force $\Delta i_{qsm}^* = 3.5$A.

3.1.2 Step load regulation response ($\Delta T_L = 1$ (N · m):

(i) maximum dip $\Delta\omega_{dm} = 15$rpm;

(ii) steady-state error = 0.

The governed equations concerning the controller parameters and the given specifications have been derived in [15], according to which the parameters of the PI-D 2DOFC can be found quantitatively and systematically. The designed results are listed as follows:

$$K_P = 75.8266 \quad K_I = 352.0745 \quad K_D = 1.8961$$
$$c_0 = 83.3072 \quad c_1 = 17.9419$$
$$d_0 = 83.3072 \quad d_1 = 9.2822 \tag{16}$$

The simulated rotor speed and torque current responses of the designed PI-D 2DOFC at various cases due to step speed command and load torque changes are shown in Figs. 5 and 6 and Figs. 7 and 8, respectively. The results indicate that the prescribed control specifications given previously are completely satisfied for the ideal IFO induction motor drive in the nominal case (i.e. $T_r = T_r^*$, $J = \bar{J}$ and $B = \bar{B}$). However, as the variations of rotor and mechanical parameters occur, the responses will deviate significantly from the desired ones. This will be improved using the proposed FRC introduced later. In that, a reference model $G_m(s)$ generating the desired speed response $\Delta\omega_{rm}$ is necessary. This can be found from Fig. 2 without adding the FRC at nominal case (i.e. neglect the uncertainty models $\Delta_I(s)$ and $\Delta G_p(s)$ and the dead-time element) and using eqn. 16:

$$G_m(s) \triangleq \frac{\Delta\omega_r}{\Delta\omega_r^*} = \frac{9.2822s + 83.3072}{s^2 + 9.128s + 83.3072} \tag{17}$$

In real applications, a step speed command with very large magnitude is usually impossible. In this case, the ramp command with suitable changing rate can be employed as an alternative. The derivation about this issue can be referred to [15].

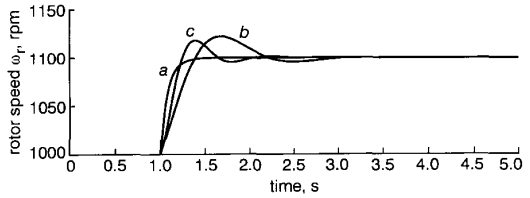

Fig. 5 *Simulated rotor speeds of PI-D 2DOFC at nominal case*
Due to step speed command change $\Delta\omega_r^* = 100$rpm
a, $T_r = 1.0\ T_r^*$, $J = \bar{J}$, $B = \bar{B}$
b, $T_r = 0.5\ T_r^*$, $J = 5\bar{J}$, $B = \bar{B}$
c, $T_r = 2.0\ T_r^*$, $J = 5\bar{J}$, $B = \bar{B}$

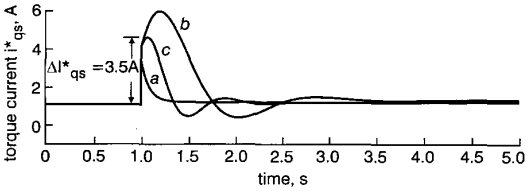

Fig. 6 *Simulated torque currents of PI-D 2DOFC at nominal case*
Due to step speed command change $\Delta\omega_r^* = 100$rpm
a, $T_r = 1.0\ T_r^*$, $J = \bar{J}$, $B = \bar{B}$
b, $T_r = 0.5\ T_r^*$, $J = 5\bar{J}$, $B = \bar{B}$
c, $T_r = 2.0\ T_r^*$, $J = 5\bar{J}$, $B = \bar{B}$

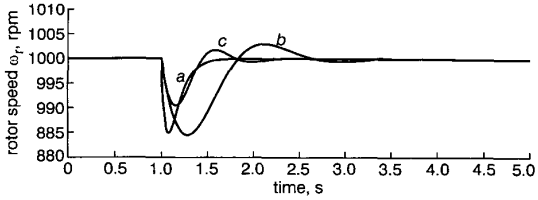

Fig. 7 *Simulated rotor speeds of PI-D 2DOFC at nominal case*
Due to step load torque change $\Delta T_L = 1$N·m
a, $T_r = 1.0\ T_r^*$, $J = \bar{J}$, $B = \bar{B}$
b, $T_r = 0.5\ T_r^*$, $J = 5\bar{J}$, $B = \bar{B}$
c, $T_r = 2.0\ T_r^*$, $J = 5\bar{J}$, $B = \bar{B}$

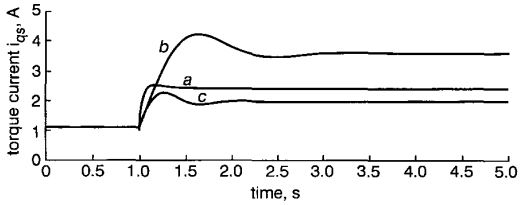

Fig. 8 *Simulated torque currents of PI-D 2DOFC at nominal case*
Due to step load torque change $\Delta T_L = 1$N·m
a, $T_r = 1.0\ T_r^*$, $J = \bar{J}$, $B = \bar{B}$
b, $T_r = 0.5\ T_r^*$, $J = 5\bar{J}$, $B = \bar{B}$
c, $T_r = 2.0\ T_r^*$, $J = 5\bar{J}$, $B = \bar{B}$

4 Proposed fuzzy robust controller

The robust technique, based on direct cancellation of uncertainties presented in [11], is easy to apply and effective in reducing the effects of system parameter variations. However, since the weighting factor set to determine the extent of disturbance compensation is fixed, it lacks control adaptability. This will lead to the performance degradation and even the stability problem over a wide operation range, especially for the system having some nonlinearities. Before introducing the proposed FRC, the conventional robust control is briefly described.

4.1 Robust controller with fixed weighting factor

The motor drive controlled by the PI-D 2DOFC and the RC with fixed weighting factor w is shown in Fig. 9. For an ideal IFO induction motor drive ($\Delta_t(s) = 0$) at the nominal case ($J = \bar{J}$ and $B = \bar{B}$), the compensation control signal $\delta i_{qs}^* = 0$. Now, suppose that the uncertainties due to nonideal field-orientation and variations of mechanical parameters occur to allow:

$$k_t \triangleq k_t^* + \Delta_t(s) \quad J \triangleq \bar{J} + \Delta J \quad B \triangleq \bar{B} + \Delta B \tag{18}$$

The dynamic behaviour of the perturbed motor drive compensation by the RC is first observed. The transfer functions of the compensated motor drive model shown in Fig. 9 can be derived to be:

$$H_{ri}(s) \triangleq \frac{\Delta\omega_r(s)}{\Delta\bar{i}_{qs}^*(s)} = \frac{k_t^* + (1-w)\Delta_t(s)/(1+w(\Delta_t(s)/k_t^*))}{\bar{J}s + \bar{B} + ((1-w)\Delta Js + (1-w)\Delta B)/(1+w(\Delta_t(s)/k_t^*))} \tag{19}$$

and

$$H_{dd}(s) \triangleq \frac{\Delta\omega_r(s)}{\Delta T_L(s)} = \frac{-(1-w)/(1+w(\Delta_t(s)/k_t^*))}{\bar{J}s + \bar{B} + ((1-w)\Delta Js + (1-w)\Delta B)/(1+w(\Delta_t(s)/k_t^*))} \tag{20}$$

the parameter w in eqns. 19 and 20 denotes a weighting factor. An equivalent motor drive control system block diagram corresponding to eqns. 19 and 20 is shown in Fig. 10. The disturbance ΔT_L and the uncertainties listed in eqn. 18 have been reduced by a factor of $(1 - w)$, $0 \le w \le 1$. For the ideal case ($w = 1$), one can find from eqns. 19 and 20 that:

$$\frac{\Delta\omega_r}{\Delta\bar{i}_{qs}^*} = \frac{k_t^*}{\bar{J}s + \bar{B}} \quad \text{and} \quad \frac{\Delta\omega_r}{\Delta T_L} = 0 \tag{21}$$

That is, all the disturbances and uncertainties have been eliminated completely by the compensation control signal δi_{qs}^*. However, this ideal case is practically unrealisable [12].

As to the performance of the compensated motor drive controlled by the designed PI-D 2DOFC and RC, the closed-loop transfer functions between $\Delta\bar{i}_{qs}^*$ to command $\Delta\omega_r^*$, and $\Delta\omega_r$ to command $\Delta\omega_r^*$ can be derived from Fig. 10 as:

$$H_{di}(s) \triangleq \frac{\Delta\bar{i}_{qs}^*(s)}{\Delta\omega_r^*(s)} = \frac{G_{3c}(s)G_{1c}(s)}{(1-w) + wG_I(s)G_p(s) + G_{2c}(s)G_p(s)k_t + G_{1c}(s)G_p(s)k_t} \tag{22}$$

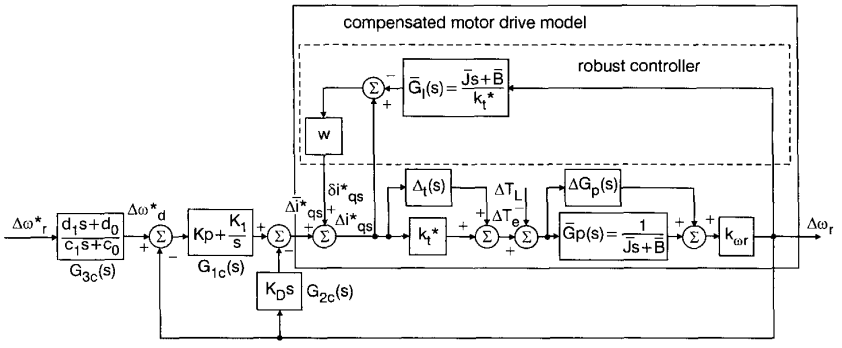

Fig. 9 *Block diagram of robust PI-D 2DOF control system*

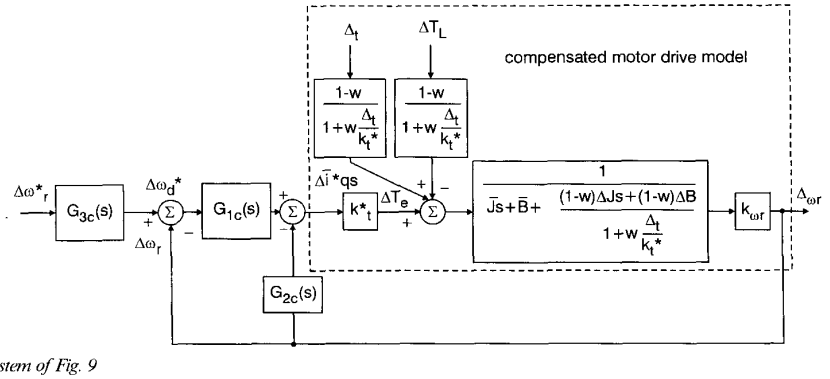

Fig. 10 *Equivalent system of Fig. 9*

$$H_{dr}(s) \triangleq \frac{\Delta\omega_r(s)}{\Delta\omega_r^*(s)} = \frac{G_{3c}(s)G_{1c}(s)G_p(s)k_t}{(1-w)+wG_I(s)G_p(s)k_t+G_{2c}(s)G_p(s)k_t+G_{1c}(s)G_p(s)k_t} \quad (23)$$

The simulated responses from eqns. 22 and 23 are plotted in Figs. 11 and 12. The results show that, as the value of w approaches 1, the control performance becomes better but subject to the increase of the control effort. So, generally, a compromise should be made in choosing the value of w.

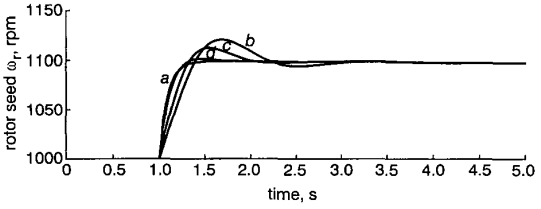

Fig. 11 *Simulated responses of uncertain motor drive controlled by PI-D 2DOFC and RC due to step command change $\Delta\omega_r^* = 100$rpm at nominal case*
Rotor speeds
$T_r = 0.5\,T_r^*$, $J = 5\bar{J}$, $B = \bar{B}$
a, reference model; *b*, $w = 0$; *c*, $w = 0.5$; *d*, $w = 0.9$

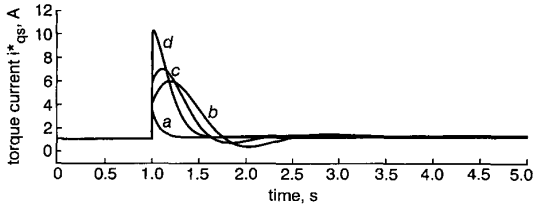

Fig. 12 *Simulated responses of uncertain motor drive controlled by PI-D 2DOFC and RC due to step command change $\Delta\omega_r^* = 100$rpm at nominal case*
Torque currents
$T_r = 0.5\,T_r^*$, $J = 5\bar{J}$, $B = \bar{B}$
a, reference model; *b*, $w = 0$; *c*, $w = 0.5$; *d*, $w = 0.9$

4.2 Proposed fuzzy robust controller

It has been observed from the previous analysis that the control performance of the RC is much affected by the chosen value of weighting factor. In addition to this. the control effort requirement and closed-loop stability are also highly dependent on the weighting factor, particularly for the system with nonlinear elements. In an inverter-fed induction motor drive, there always exists some transport lag, or so-called dead time. It is yielded mainly due to the inverter blanking time, inaccurate inverter current switching control, coupling of rotor shaft and the speed sampling instants being not synchronised with the encoder pulses.

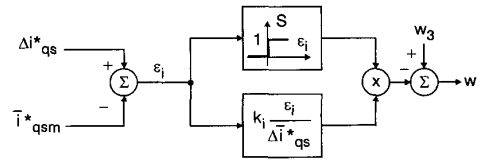

Fig. 15 *Configuration of control force compromising scheme*

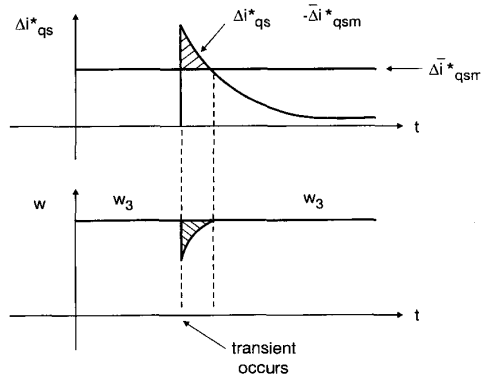

Fig. 16 *Operation principle of control force compromising scheme*

To overcome the problems mentioned above, a fuzzy robust controller is proposed in Fig. 13. The fuzzy weighting controller (Figs. 14–16) adaptively tunes the weighting factor of the RC according to the model following error and control effort (Δi_{qs}^*), such that the desired control performance is obtained. In addition, for enhancing the closed-loop control stability, the drive system dead-time element $N_d(s)$ and the corresponding simple dead-time

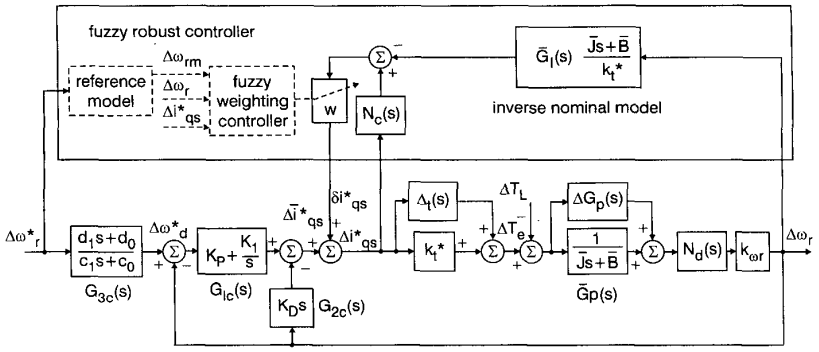

Fig. 13 *Block diagram of proposed FRC*

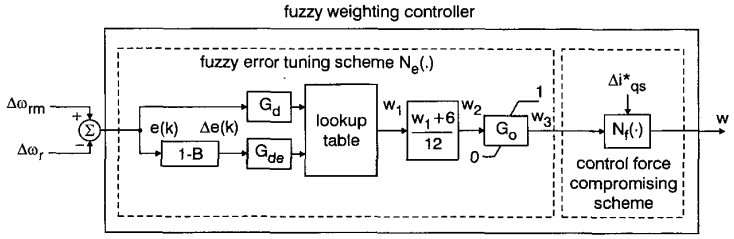

Fig. 14 *Configuration of proposed fuzzy weighting controller*

compensator (DTC) $N_c(s)$ [11, 12] are included in Fig. 13. The effectiveness of $N_c(s)$ is first observed. By supposing the fixed value of w, the closed-loop command tracking transfer function without and with $N_c(s)$ can be derived from Fig. 13 to be:

Without $N_c(s)$:

$$H_{dr}(s) \triangleq \frac{\Delta\omega_r(s)}{\Delta\omega_r^*(s)} = \frac{G_{3c}(s)G_{1c}(s)G_p(s)k_t}{(1-w)e^{\tau_d s}+wG_I(s)G_p(s)k_t+G_{2c}(s)G_p(s)k_t+G_{1c}(s)G_p(s)k_t} \triangleq \frac{N_1(s)}{D_1(s)} \tag{24}$$

With $N_c(s)$:

$$H_{drc}(s) \triangleq \frac{\Delta\omega_r(s)}{\Delta\omega_r^*(s)} = \frac{G_{3c}(s)G_{1c}(s)G_p(s)k_t}{e^{\tau_d s}-we^{(\tau_d-\tau_c)}+wG_I(s)G_p(s)k_t+G_{2c}(s)G_p(s)k_t+G_{1c}(s)G_p(s)k_t} \triangleq \frac{N_2(s)}{D_2(s)} \tag{25}$$

By approximating the dead-time element $e^{-\tau s}(\tau = \tau_d \text{ or } \tau_c)$ with:

$$e^{-\tau s} = \frac{1-\tau s/2}{1+\tau s/2} \tag{26}$$

the numerators and denominators in eqns. 24 and 25 can be expressed as:

$$N_1(s) = k_t^*(d_1 s + d_0)(k_P s + k_I)(k_t^* + \Delta_t)(1 - \tau_d s/2) \tag{27}$$

$$\begin{aligned} D_1(s) &= \{[(1-w)(Js+B)(1+\tau_d s/2)(c_1 s + c_0)k_t^* s] \\ &+ [w(\overline{J}s + \overline{B})(k_t^* + \Delta_t)(1-\tau_d s/2)(c_1 s + c_0)s] \\ &+ [(k_D s^2 + k_P s + k_I)(k_t^* + \Delta_t)(1-\tau_d s/2) \\ &\cdot (c_1 s + c_0)k_t^*]\} \end{aligned} \tag{28}$$

$$N_2(s) = k_t^*(d_1 s + d_0)(k_P s + k_I)(k_t^* + \Delta_t) \cdot (1 - \tau_d s/2)(1 - \tau_d s/2 + \tau_c s/2) \tag{29}$$

$$\begin{aligned} D_2(s) &= \{[(1+\tau_d s/2)(Js+B)(1-\tau_d s/2+\tau_c s/2)k_t^* s] \\ &- [w(1-\tau_d s/2)(1+\tau_d s/2-\tau_c s/2) \\ &\cdot (Js+B)(c_1 s + c_0)k_t^* s] + [w(\overline{J}s + \overline{B}) \\ &\cdot (k_t^* + \Delta_t)(1-\tau_d s/2)(1-\tau_d s/2+\tau_c s/2) \\ &\cdot (c_1 s + c_0)s] + [(k_D s^2 + k_P s + k_I)(k_t^* + \Delta_t) \\ &\cdot (1-\tau_d s/2)(1-\tau_d s/2+\tau_c s/2)(c_1 s + c_0)k_t^*]\} \end{aligned} \tag{30}$$

Generally, the dead-time τ_d can be estimated experimentally, and, accordingly, τ_c can be determined. Now, under the assumption of $\tau_c = \tau_d = 0.02$s, the inertia constant J is varied from $\bar{J}$ toward $5\bar{J}$ and $T_r = T_r^*$, $0.5T_r^*$, $2T_r^*$, the parameter plane (w against J) representing the stability limits of the closed-loop system shown in Fig. 13 without and with the DTC is plotted in Fig. 17. The stability analyses made in Fig. 17 indicate that, by adding the DTC, the weighting factor w can be chosen larger (up to 1 here) to yield better control performance.

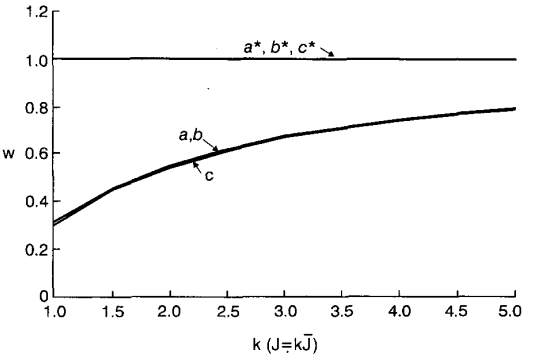

Fig. 17 *Closed-loop stability limits of motor drive controlled by RC with and without DTC*
a*, with DTC, $T_r = 1.0\ T_r^*$ — *a*, without DTC, $T_r = 1.0\ T_r^*$
*b**, with DTC, $T_r = 0.5\ T_r^*$ — *b*, without DTC, $T_r = 0.5\ T_r^*$
*c**, with DTC, $T_r = 2.0\ T_r^*$ — *c*, without DTC, $T_r = 2.0\ T_r^*$

Fuzzy weighting controller: Detailed configuration of the proposed fuzzy weighting controller is shown in Fig. 14, in which a fuzzy error tuning scheme $N_e(\cdot)$ and a control force compromising scheme $N_f(\cdot)$ are used to handle the model following control and control effort compromise tasks, respectively.

Fuzzy error tuning scheme: To allow the RC possess adaptive capability, it is proposed that the weighting factor of the RC is adaptively tuned by the fuzzy error tuning scheme, which is driven by a model following error, and its change defined as $e(k) \triangleq \Delta\omega_{rm}(k) - \Delta\omega_r(k)$ and $\Delta e(k) \triangleq (1 - B)e(k) = e(k) - e(k-1)$ with $\Delta\omega_{rm}(k)$ and $\Delta\omega_r(k)$ being the responses of the reference model and the rotor speed at kth sampling interval, respectively. The major purpose of the proposed controller is to allow the resulting motor speed tracking response to closely follow those of the reference model. Thus the general model following the error trajectory can be predicted and plotted in Fig. 18, in which, some indices are defined for the convenience of making dynamic signal analysis: $c_i \triangleq$ reference crossover point, $m_i \triangleq$ reference extreme point and $A_i \triangleq$ reference range. The membership functions used here are sketched in Fig. 19, where the fuzzy numbers are PB, PM, PS, ZE, NS, NM, NB. Incorporating these fuzzy numbers, the numbers of quantisation levels of the input variables $e(k)$ and $\Delta e(k)$ are chosen to be 13 and are listed in Table 1 (The scaling is set as 1V to 1000rpm). To increase the sensitivities, $e(k)$ and $\Delta e(k)$ are properly scaled by factors G_e and Gde, respectively. G_e and G_{de} are chosen to be 20 and 0.1 here, respectively.

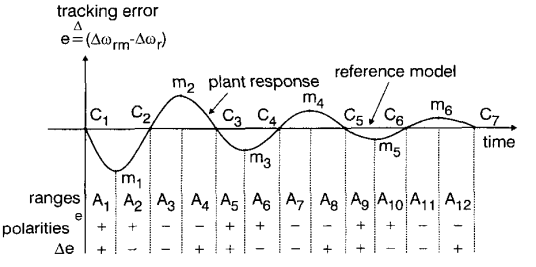

Fig. 18 *General model reference tracking error dynamic behaviour*

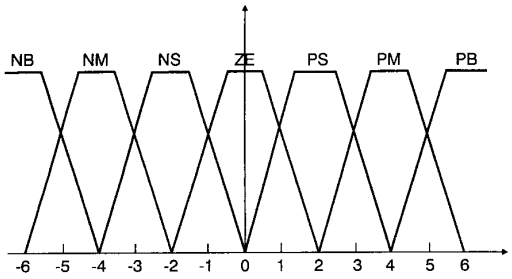

Fig. 19 *Chosen membership functions*

Table 1: Quantised error and error change

error e (V)	error change Δe (V)	quantized level
$e \le -1.6$	$\Delta e \le -1.6$	–6
$-1.6 < e \le -0.8$	$-1.6 < \Delta e \le -0.8$	–5
$-0.8 < e \le -0.4$	$-0.8 < \Delta e \le -0.4$	–4
$-0.4 < e \le -0.2$	$-0.4 < \Delta e \le -0.2$	–3
$-0.2 < e \le -0.1$	$-0.2 < \Delta e \le -0.1$	–2
$-0.1 < e \le -0.05$	$-0.1 < \Delta e \le -0.05$	–1
$-0.05 < e \le 0.05$	$-0.05 < \Delta e \le 0.05$	0
$0.05 < e \le 0.1$	$0.05 < \Delta e \le 0.1$	1
$0.1 < e \le 0.2$	$0.1 < \Delta e \le 0.2$	2
$0.2 < e \le 0.4$	$0.2 < \Delta e \le 0.4$	3
$0.4 < e \le 0.8$	$0.4 < \Delta e \le 0.8$	4
$0.8 < e \le 1.6$	$0.8 < \Delta e \le 1.6$	5
$1.6 < e$	$1.6 < \Delta e$	6

Table 2: Linguistic rules of fuzzy error tuning scheme

e / Δe / w_1	NB	NM	NS	ZE	PS	PM	PB
NB	NB	NB	NB	NB	NM	NS	ZE
NM	NB	NB	NB	NM	NS	ZE	PS
NS	NB	NB	NM	NS	ZE	PS	PM
ZE	NB	NM	NS	ZE	PS	PM	PB
PS	NM	ZS	NS	PS	PM	PB	PB
PM	NS	ZE	PS	PM	PB	PB	PB
PB	ZE	PS	PM	PB	PB	PB	PB

Table 3: Tracking decision lookup table

e / Δe / w_1	–6	–5	–4	–3	–2	–1	0	1	2	3	4	5	6
–6	–6	–6	–6	–6	–6	–6	–6	–5	–4	–3	–2	–1	0
–5	–6	–6	–6	–6	–6	–6	–5	–4	–3	–2	–1	0	1
–4	–6	–6	–6	–6	–6	–5	–4	–3	–2	–1	0	1	2
–3	–6	–6	–6	–6	–5	–4	–3	–2	–1	0	1	2	3
–2	–6	–6	–6	–5	–4	–3	–2	–1	0	1	2	3	4
–1	–6	–6	–5	–4	–3	–2	–1	0	1	2	3	4	5
0	–6	–5	–4	–3	–2	–1	0	1	2	3	4	5	6
1	–5	–4	–3	–2	–1	0	1	2	3	4	5	6	6
2	–4	–3	–2	–1	0	1	2	3	4	5	6	6	6
3	–3	–2	–1	0	1	2	3	4	5	6	6	6	6
4	–2	–1	0	1	2	3	4	5	6	6	6	6	6
5	–1	0	1	2	3	4	5	6	6	6	6	6	6
6	0	1	2	3	4	5	6	6	6	6	6	6	6

Based on the experience about the motor drive to be controlled and the properties of dynamic signal analyses made in [9], the linguistic rules of the fuzzy error tuning scheme are decided and listed in Table 2. By using the centre-of-gravity (COG) method, a decision lookup table is then constructed in Table 3. To let the value of weighting factor be located in the range 0~1, and to enhance the error driven adaptive capability, the output (w_1) from lookup table is processed according to:

$$w_3 = G_0 w_2 = G_0 \left(\frac{w_1 + 6}{12} \right) \tag{31}$$

where the model following error dependent gain function is defined as:

$$G_0 = \begin{cases} 0 & \text{for } |e| < e_{r0} \\ k_1(|e| - e_{r0}) & \text{for } |e| \ge e_{r0} \end{cases} \tag{32}$$

with $e_{r0} = 0.002$ V and $k_1 = 50$ being set.

Control force compromising scheme: Having generated the weighting factor w_3 from the fuzzy error tuning scheme, which is designed emphasised in obtaining a good model following response the proposed control force compromising scheme is further used to make the compromise between performance and control effort. Detailed configurations and operating principles of the proposed control force compromising scheme are shown in Figs. 15 and 16. From Figs. 15 and 16 it can be seen that the weighting factor will be forced towards a smaller value, as the control effort (Δi_{qs}^*) is larger than the preset value $\Delta \bar{i}_{qsm}^*$ ($\ge \Delta i_{qsm}^*$ which is set in the design of PI-D 2DOFC). The parameter k_i in Fig. 15 is used to adjust the extent of control force compromise. In this paper, $k_i = 5$ is set.

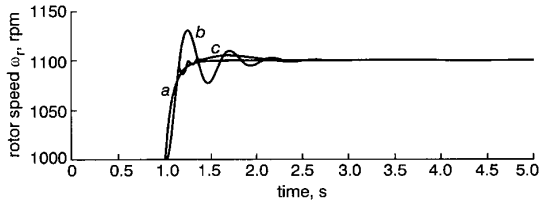

Fig. 20 *Simulated responses at $J = 5\bar{J}$, $T_r = 0.5T_r^*$, $\tau_d = \tau_c = 0.02$s without current limitation*
Rotor speed responses due to command change
a, reference model
b, RC with DTC and fixed $w = 1.0$
c, proposed FRC

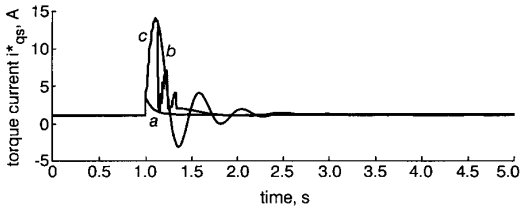

Fig. 21 *Simulated responses at $J = 5\bar{J}$, $T_r = 0.5T_r^*$, $\tau_d = \tau_c = 0.02$s without current limitation*
Torque current responses due to command change
a, reference model
b, RC with DTC and fixed $w = 1.0$
c, proposed FRC

4.3 Simulation and experimental results

From the stability analysis made in Fig. 17 one can find that, if the DTC is added, the weighting factor w can be set up to 1 under the condition: $J = 5\bar{J}$, $T_r = 0.5T_r^*$, $\tau_c = \tau_d = 0.02$s. The simulated rotor speed ω_r and torque current i_{qs}^* due to speed command changed from 1000rpm to 1100rpm by this RC without control force limitation are shown in Figs. 20 and 21. For the same case, the simulated

results of the proposed FRC accompanied by the desired reference responses are also shown in Figs. 20 and 21. As to the regulation characteristics, the simulated responses due to the load torque change of 1N·m in a nominal case are compared in Figs. 22 and 23. The results in Figs. 20–23 indicate that the proposed FRC yields better tracking and regulation control performances. Now let $\Delta \bar{i}^{*}_{qsm}$ in the proposed control force compromising scheme be $\Delta \bar{i}^{*}_{qsm}$ = 6A, the simulated response of the proposed FRC at the same condition as those of Figs. 20–23 are shown in Figs. 24 and 25. For comparison, the simulated responses of RC with fixed weighting factor w = 1 and hard current limit = 8A are compared in Figs. 24 and 25. Better compromised responses are also obtained by the proposed FRC.

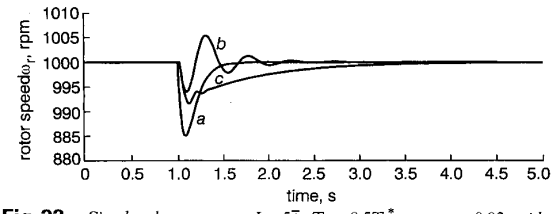

Fig. 22 *Simulated responses at $J = 5\bar{J}$, $T_r = 0.5T_r^*$, $\tau_d = \tau_c = 0.02$s without current limitation*
Rotor speed responses due to load torque change of ΔT_L = 1N·m
a, reference model
b, RC with DTC and fixed w = 1.0
c, proposed FRC

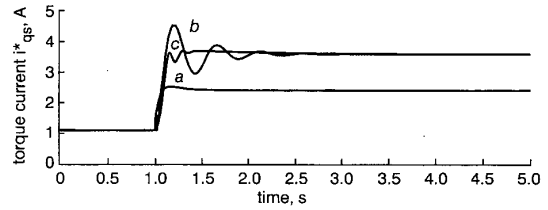

Fig. 23 *Simulated responses at $J = 5\bar{J}$, $T_r = 0.5T_r^*$, $\tau_d = \tau_c = 0.02$s without current limitation*
Torque current responses due to load torque change of ΔT_L = 1N·m
a, reference model
b, RC with DTC and fixed w = 1.0
c, proposed FRC

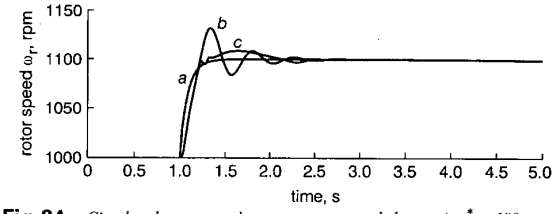

Fig. 24 *Simulated responses due to step command change $\Delta\omega_r^* = 100$rpm at $J = 5\bar{J}$, $T_r = 0.5T_r^*$, $\tau_d = \tau_c = 0.02$s with current limitation*
Rotor speeds
a, reference model
b, RC with DTC and current limitation (w = 1.0)
c, proposed FRC with current limitation

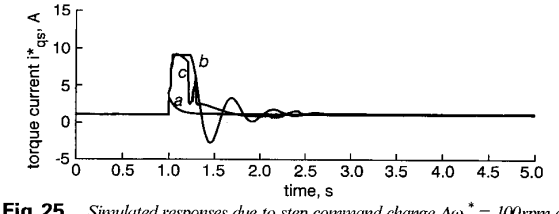

Fig. 25 *Simulated responses due to step command change $\Delta\omega_r^* = 100$rpm at $J = 5\bar{J}$, $T_r = 0.5T_r^*$, $\tau_d = \tau_c = 0.02$s with current limitation*
Torque currents
a, reference model
b, RC with DTC and current limitation (w = 1.0)
c, proposed FRC with current limitation

The designed controller is transformed into digital control algorithms using C-language and executed on a PC 486-based control computer with necessary interfacing cards. Some experimental results are given for further demonstrating the effectiveness of the proposed fuzzy robust controller. The measured results (not shown here) at nominal case have confirmed that the given control specifications are fully satisfied. For verifying the robustness of the proposed FRC under large drive parameter variations, the flux current command and the rotor resistance set in the IFO mechanism are changed from i_{ds}^* = 3.3A to 1.65A and R_r = 1.3Ω to 1.58Ω, and a mass of 3.78kg (ΔJ = 1.04009N·m·s·rad/V) is added to the rotor shaft to let $J = \bar{J}$ = 1.4815N·m·s·rad/V be changed to J = 2.52159N·m·s·rad/V($J = 1.7\bar{J}$). The measured rotor speeds and torque currents of the motor drive controlled by the PI-D 2DOFC due to command change from 1000rpm to 1100rpm (R_L = 77.6Ω) and load resistance change from R_L = 77.6Ω to 27.4Ω (ω_{r0} = 1000rpm) are plotted in Figs. 26

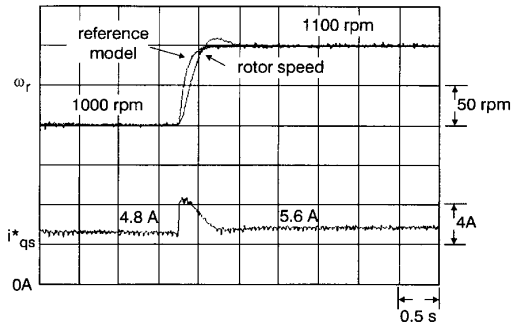

Fig. 26 *Measured rotor speeds and torque currents of detuned IFO induction motor drive with $J = 1.7\bar{J}$ controlled by PI-D 2DOFC*
Due to step command change from 1000rpm to 1100rpm (R_L = 77.6Ω)

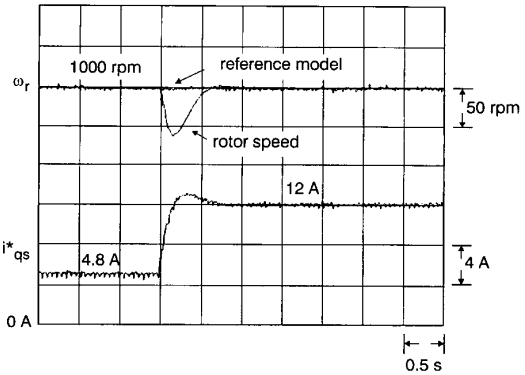

Fig. 27 *Measured rotor speeds and torque currents of detuned IFO induction motor drive with $J = 1.7\bar{J}$ controlled by PI-D 2DOFC*
Due to step load resistance change from R_L = 77.6Ω to 27.4Ω (ω_r = 1000rpm)

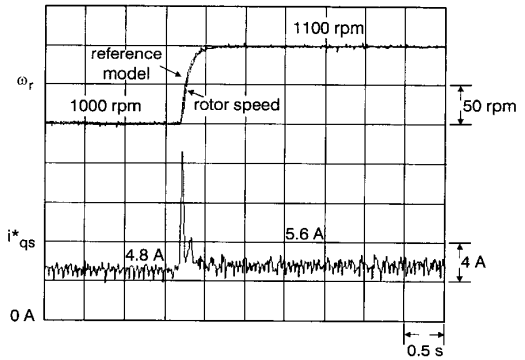

Fig. 28 *Measured rotor speeds and torque currents of detuned IFO induction motor drive controlled by proposed FRC at the same conditions as Fig. 26*
Tracking without control force compromising scheme

and 27. At the same condition, the measured results of the designed FRC without and with control force compromise ($\Delta \bar{i}^{*}_{qsm}$ = 6A) due to command changed from 1000rpm to 1100rpm are shown in Figs. 28 and 29. The measured responses of the designed FRC due to the load resistance changed from R_L= 77.6Ω to 27.4Ω are shown in Fig. 30. The results shown in Figs. 26–30 confirm that good tracking and regulation control responses are obtained by the proposed FRC.

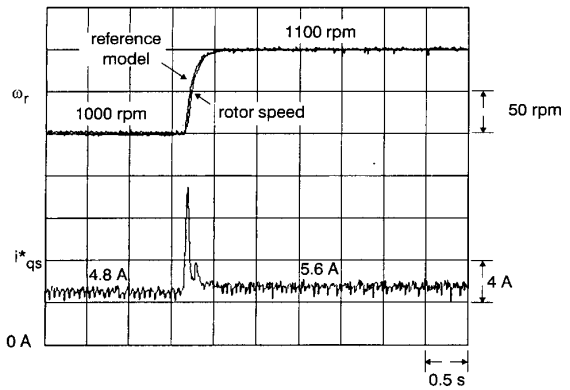

Fig.29 *Measured rotor speeds and torque currents of detuned IFO induction motor drive controlled by proposed FRC at the same conditions as Fig. 26*
Tracking with control force compromising scheme

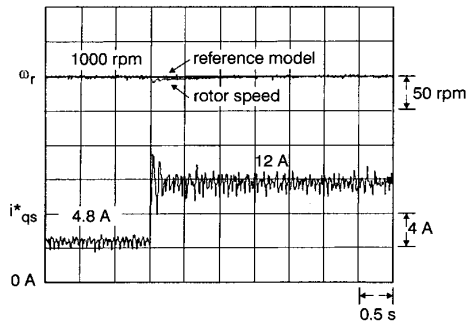

Fig.30 *Measured rotor speeds and torque currents of detuned IFO induction motor drive controlled by proposed FRC at the same conditions as Fig. 26*
Regulation

5 Conclusions

A fuzzy robust controller for improving the performance of a detuned IFO induction motor drive has been presented. For the convenience of controller analysis and design, the transfer function model of a detuned IFO induction motor drive is established. By neglecting the system dead-time and uncertainties, a PI-D 2DOFC is designed at nominal case to match the prescribed tracking and regulation speed responses, and a reference model representing the desired tracking response is determined. Then having analysed the stability and robustness of the traditional robust controller, a fuzzy robust controller is proposed. The major features of the proposed FRC lie in: (i) since its weighting factor is adaptively tuned using a fuzzy error tuning scheme, better speed model following response is obtained; and (ii) the compromise between the performance and control force is automatically considered by the proposed control force compromising scheme. The simulation and experimental results have demonstrated that good control performances both in command tracking and load regulation are achieved by the proposed FRC, and moreover, the performances are rather insensitive to the operating condition changes.

6 References

1 BOSE, B. K.: 'Power electronics and AC drives' (Prentice-Hall, 1986)
2 NOVOTNY, D.W., and LIPO, T.A.: 'Vector control and dynamics of AC drives' (Clarendon Press, Oxford, 1996)
3 KRISHNAN, R., and DORAN, F.C.: 'Study of parameter sensitivity in high-performance inverter-fed induction motor drive systems', *IEEE Trans.*, 1987, **IA–23**, (4), pp. 623–635
4 KRISHNAN, R., and BHARADWAJ, A.S.: 'A review of parameter sensitivity and adaptation in direct under vector controlled induction motor drive systems', *IEEE Trans.*, 1991, **PE–6**, (4), pp. 695–703
5 ROBYNS, B., BUYSE, H., and LABRIQUE, F.: 'Influence of parameter uncertainties on the performance of some induction actuator indirect field orientated control scheme', *IEEE Soc. Ind. Appl.*, 1993, pp. 79–84
6 LIAW, C.M., WANG, J.B., and CHANGE, Y.C.: 'A fuzzy adapted field-orientated mechanism for induction motor drive', *IEEE Trans.*, 1996, **EC–11**, (1), pp. 76–83
7 PARK, M.H., and KIM, K.S.: 'Chattering reduction in the position control of induction motor using the sliding mode', *IEEE Trans.*, 1991, **PE–6**, (3), pp. 317–325
8 CERRUTO, E., CONSOLI, A., RACITI, A., and TESTA, A.: 'Fuzzy adaptive vector control of induction motor drive', *IEEE Trans.*, 1997, **PE–12**, (6), pp. 1028–1039
9 KUNG, Y.S., and LIAW, C.M.: 'A fuzzy controller improving a linear model following controller for motor drives', *IEEE Trans.*, 1994, **FS–2**, (3), pp. 194–202
10 BA-RAZZOUK, A., CHERITI, A., OLIVIER, G., and SICARD, P.: 'Field-orientated control of induction motors using neural-network decouplers', *IEEE Trans.*, 1997, **PE–12**, (4), pp. 752–763
11 LIAW, C.M., and LIN, F.J.: 'Control of indirect field-orientated induction motor drives considering the effects of dead-time and parameter variations', *IEEE Trans.*, 1993, **IE–40**, (5), pp. 486–495
12 HONG, K., and NAM, K.: 'A load torque compensation scheme under the speed measurement delay', *IEEE Trans.*, 1998, **IE–45**, (2), pp. 283–290
13 WANG., J.B.: 'Controls for improving the decoupling characteristic and speed response of an indirect field-orientated induction motor drive'. PhD thesis, Department of EE, Tsing Hua University, 1997
14 LIAW, C.M.: 'System parameter estimation from sampled data', *Contr. Dyn. Syst.*, 1994, **63**, pp. 161–175
15 LIAW, C.M., CHEN, Y.K., CHAO, K.H., and CHEN, H.C.: 'Quantitative design and implementation of PI-D controller with model-following response for motor drive', *IEE Proc., Electr. Power Appl.*, 1997, **145**, (2), pp. 98–104